STM JOURNALS

Journal of
Polymer & Composites

ISSN: 2321-2810 (Online)
ISSN: 2321-8525 (Print)
Volume 11, Special Issue 2, 2023
DOI (Journal): 10.37591/JoPC

http://engineeringjournals.stmjournals.in/index.php/JoPC/index

Research JoPC

Study of Electrochemical and Mechanical Properties of Graphene/HAp Composite Coating on Ti-13Nb-13Zr Alloy via Electrophoretic Deposition for Biomedical Application

Nabeel Mohammed Abd Alkadim[1,*], Jassim Mohammed Salman[2]

Abstract

Titanium-13niobium-13zirconium alloy has widespread potential in biomedical applications due to its high degree of biocompatibility, favourable mechanical properties, high corrosion resistance, and high possibility of osseointegration. The surface was improved by electrophoretic deposition method using hydroxyapatite and graphene (5 g nanoHAp) (5 g nanoHAp+0.06 nanoGr) and suspended in ethanol solution at different conditions of time (1, 3, and 7 minutes) and voltage (50, 70, and 100 V). The effect of the two suspended materials on the surface of the Ti-13Nb-13Zr alloy was studied by using the tests of visual observation, scanning electron microscopy (SEM), and the weight and thickness of the coating layer to know the homogeneity of the coating layer, and adhesion testing, contact angle, wear test and electrochemical tests in addition to X-ray diffraction. The results showed that the addition of graphene led to the stability of the coating layer thickness with deposition time in contrast to the voltage and an improvement in the adhesion, which increased from 0.91 to 3.03 compared to adding hydroxyapatite only. The corrosion strength was improved from 76% for hydroxyapatite coating at 1 minute and 70 V to 95% for graphene-hydroxyapatite coating under the same conditions. When tested for wear, lower volume loss is evident for the graphene-hydroxyapatite coating compared to the hydroxyapatite coating under the same condition.

Keywords: Corrosion behaviour, electrophoretic deposition, Ti-13Nb-13Zr alloy, hydroxyapatite, graphene

INTRODUCTION

A biomaterial is a natural or synthetic substance that is employed to substitute or perform bodily functions. The biological systems of the body may communicate with the biomaterial. A biomaterial called a biocomposite is created by mixing several kinds of materials to achieve the necessary qualities and satisfy the requirements for use as a biomaterial. With their biocompatible, non-toxic, anti-inflammatory, and bioactive qualities, biocomposites for metallic implants produced from bioceramic and biopolymer are being developed in an effort to avoid infection that frequently occur during surgery and as a potential material to cure damage to teeth and bones [1]. Metallic supports that are in direct touch with the bone are used in implants. Its excellent mechanical characteristics and low density (4.5 g/cm^3) make titanium an ideal material to be utilized in alloys to create implantation. Ti-6Al-4V and CP titanium have been

***Author for Correspondence**
Nabeel Mohammed Abd Alkadim
E-mail: nabeelmohammed666@gmail.com

[1]Professor, PHD. University of Babylon, College of Materials Engineering, Hilla-Babylon, 51001, Hilla-IRAQ
[2]Professor, (PHD), University of Babylon, College of Materials Engineering, Hilla-Babylon, 51001, Hilla-IRAQ

Received Date: December 08, 2022
Accepted Date: January 31, 2023
Published Date: April 18, 2023

Citation: Nabeel Mohammed Abd Alkadim, Jassim Mohammed Salman. Study of Electrochemical and Mechanical Properties of Graphene/HAp Composite Coating on Ti-13Nb-13Zr Alloy via Electrophoretic Deposition for Biomedical Application. Journal of Polymer & Composites. 2023; 11(Special Issue 2): S91–S106.

widely used for biomedical implants throughout the last 10 years. The toxic impact of aluminium and vanadium ions released from (α + β) try typing Ti-6Al-4V alloy and the mismatch between the elasticity modulus of Ti-6Al-4V alloy (~120 GPa) and the human hard tissues (~30 GPa) that also creates stress shielding, have, nevertheless, been linked to some health issues, including neural disorder, Alzheimer's disease, and osteomalacia [2, 3]. Ti-13Zr-13Nb alloy was selected for this study because it has no toxic components and has a low Young's modulus (76 GPa), which is comparable to cortical bone and allows for improved stress distribution at the implantation-bone contact zone and prevents implantation damage and loosening. Surface molecules and atoms may be chemically or physically changed, or a layer could be deposited on the surface's top to modify it [4]. It may be a thin layer of ceramics, an organic layer, or another substance. A range of surface modification methods are shown in Figure 1. Based on the substrate's surface and the demands of the alteration, a particular strategy might be applied [5].

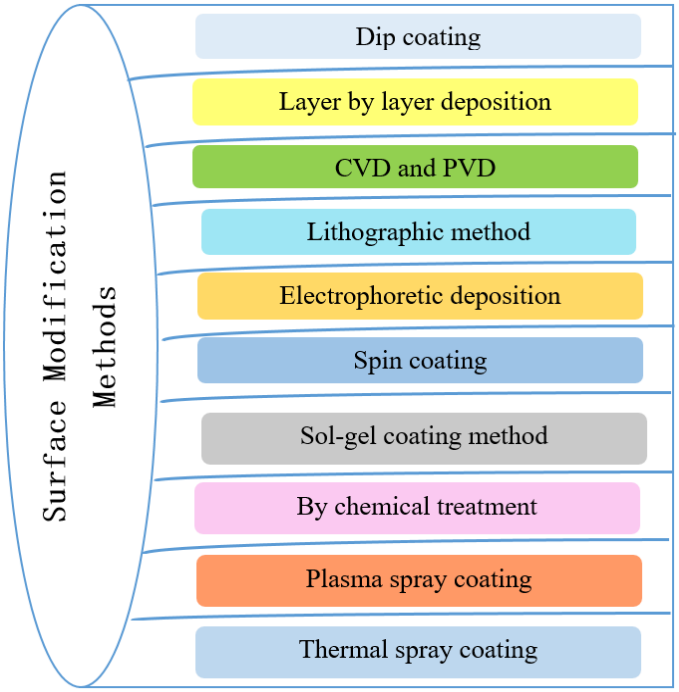

Figure 1. Schematic diagram showing different surface modifications [5].

This research used the electrophoretic deposition (EPD) method, an electrical technology that combines electrophoresis and deposition procedures. The first approach creates an electric field across two electrodes, causing particles in a suitable solution to charge up and migrate towards the electrode of the opposite charge. The particles clump together at the deposition electrode, forming a rather uniform and homogenous coating in the second step, as shown in Figure 2 [6, 7].

This technology allows for creating one-of-a-kind nanostructures and microstructures, also, innovative and complicated material mixtures in a wide range of macroscopic forms, arrangements, and dimensions, ranging from microns to nanometers. If the colloidal suspension of metals, polymers, ceramics, and glass is deposited in a small powder (less than 30 μm), it may readily be used in the EPD. The deposit must next be heat-treated to eliminate porosity and densify it [6, 8]

$Ca_{10}(PO_4)_6(OH)_2$ hydroxyapatite (HAp) nanoparticles (Figure 3a) is a naturally found calcium apatite, which makes up a significant portion of human teeth and bones. One of the popular bioceramics utilized as a bone graft alternative, this could form connections with organic compounds on its own. Because of the combination of outstanding features, including bioactivity, biocompatibility, osteoconductivity, non-inflammatory characteristics, and mechanical capabilities, as well as its distinct

chemical composition and crystal arrangement, it is widely used in biomedical applications [9, 10]. The HAp coating might well be strengthened with a material with strong mechanical properties, including graphene (Gr), to make it suitable for use in the physiological milieu of the body under intense mechanical stress. It was also claimed that Gr increases the corrosion resistance of the HAp coating. It is believed that composite coatings, including HAp-carbon, provide such a unique technique to make up for HAp's low mechanical properties (Figure 3b) [11].

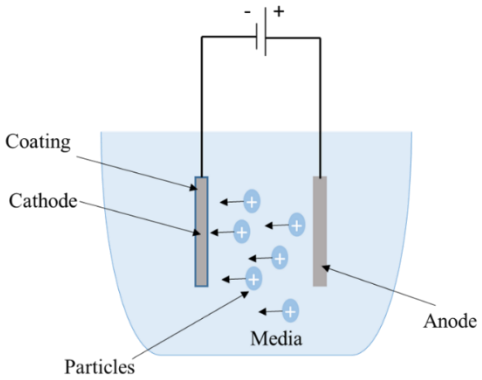

Figure 2. A cell for electrophoretic deposition (EPD) showing suspended positively charged particles migrate towards the negative electrode [7].

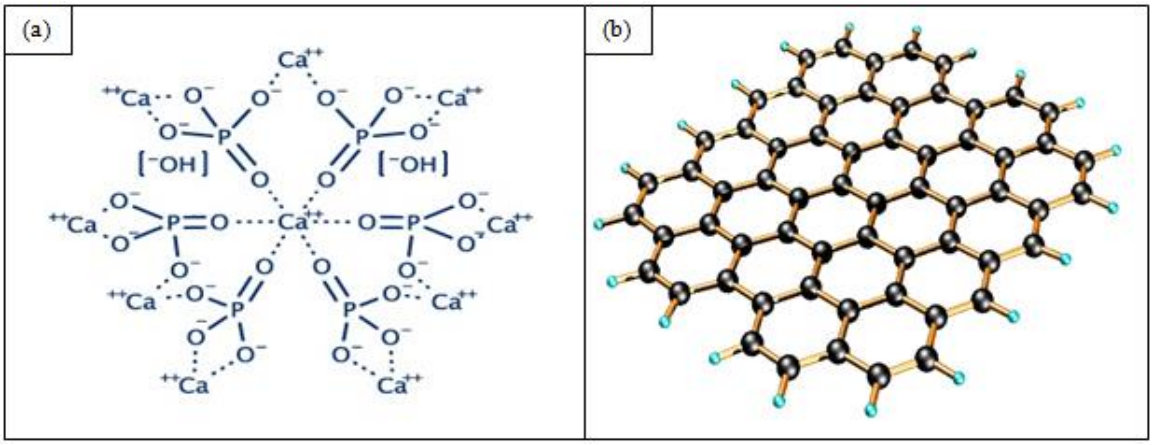

Figure 3. The crystalline structure of (a) hydroxyapatite (HAp) and (b) graphene (Gr) [12, 13].

Utilizing EPD to construct and enhance the surface of different biomedical alloys has been the subject of several papers. Bartmanski et at. [14] studied the mechanical, chemical, physical, and microstructure characteristics of thin nanohydroxyapatite coatings for Ti-13Zr-13Nb alloy concentrated on the impacts of EPD voltage for nanohydroxyapatite coating (15 and 30 V) and nanosilver decoration of nanoHAp coatings (60 V and a deposition time of 5 minutes). For the Ti-13Nb-13Zr alloy, Moskalewicz et al. [15] examined the microstructure and coating characteristics for EPD of composite alumina/polyetheretherketone (Al_2O_3/PEEK) coatings. Singh et al. [16] found that the Ti-13Nb-13Zr alloy was electrophoretically coated (EPD) with pure hydroxyapatite (HA), pure iron oxide (Fe_3O_4), and HA-Fe_3O_4-chitosan (Cs) coatings by altering the amount of Fe_3O_4 at three various levels (1, 3 and 5 wt%). Transmission and scanning electron microscopy exploration of the coating microstructure reported the existence of uniformly distributed Al_2O_3 and their agglomerates within the PEEK matrix.

In this study, the nanohydroxyapatite coating layer was improved using graphene nanoparticles with different EPD conditions (time 1, 3, 5 and 7 minutes) (voltage 50, 70, 90 and 100 V) on the surface of the Ti-13Zr-13Nb alloy and microstructural, chemical and mechanical tests were performed to determine in vitro the compatibility of the new coating layer with human body cells.

MATERIALS AND METHODOLOGY

Materials

Preparation of Specimens

Ti-13Nb-13Zr samples were cut in diameters 13 mm × 5 mm in height and abraded using silicon carbide (SiC) papers (180–1000 grits) in this investigation (composition of the Ti-13Nb-13Zr alloy is given in Table 1). They were then cleaned in an ultrasonic bath with water and acetone for 10 minutes per case, rinsed with distilled water, dried by forced air, and used as a cathode in an electrolytic cell. An aqueous solution of acetic acid (CH3COOH; 9 mL) was used as an electrolyte. The anodic oxidation process was conducted at a voltage of 15 V; the anodic duration was 5 minutes, at a temperature of ~25°C. Then, the samples were immersed for 10 minutes in 50 mL of nitric acid (HNO_3) per 100 mL. In the end, specimens were washed in distilled water, then in acetone, and finally dried in laboratory air.

Table 1. Nominal chemical composition of the Ti-13Nb-13Zr alloy utilized for the current study.

Elements	Requirements	Results
Zr	13.15	14.22
Nb	12.99	13.51
Fe	0.25	0.115
C	0.08	0.005
N	0.05	0.010
O	0.15	0.053
H	0.012	0.001
Ti	Remainder	Remainder
Residual element	0.400	0.342

Suspension Preparations

The suspension was formed by dissolving 0.5 g/L of chitosan (MW = 80 kDa) in 1 L of water. In 1% acetic acid >98% purity, it was added to 250 mL of ethanol with purity >99%. Quantities of graphene were used in different proportions (0.06, 0.2, 0.5, and 1 g) with a fixed percentage of hydroxyapatite (5 g); depending on the best results, the ratio of graphene (0.06 g) was adopted as shown in Table 2. These quantities were gradually added to the solution during mixing. To prevent evaporation, the suspension was covered with Parafilm. To break down the agglomerates, the solution was swirled for 24 hours in a magnetic stirrer and then for 20 minutes in an ultrasonic stirrer. To make a stable suspension, a homogenous dispersion of the particles was obtained and aged for 24 hours to allow full charging of the dispersed particles. The suspension was stirred for additional 10 minutes before use.

Table 2. The concentration of nano HAp) and nano Hap–nano Gr used in the coating for this study depending on the best results.

No.	Component coating	Nano HAp	Nano Gr
(a)	Nano HAp	5 g/L	-
(b)	Nano Hap–nano Gr	5 g/l	0.06 g/L

Methods

EPD Experimentation Procedure

The counter electrodes (anode) were made of 316LSS, and the substrate (Ti-13Nb-13Zr) was applied as the cathode. The electrodes were cleaned and dried with acetone. The electrodes were immersed vertically in a 250 mL beaker having the suspension. The EPD cell's gap between the electrodes was kept constant at 10 mm.

Using a laboratory DC-power source, EPD was tested at 50, 70, and 100 V. (NO: PH 2021042900, Freq: 50 Hz ± 20%, AC IN: 220 V ± 15%, and DC OUT: 150 V 10 A) (China) and various deposit durations from 1, 3, and 7 minutes and the deposition duration was recorded by a timer. The deposition process was performed on Ti-13Nb-13Zr alloy by EPD at room temperature. After the EPD processing

was completed, the samples were dried overnight in the air. EPD was carried out for each condition three times, with the average deposition computed. The apparatus used in EPD coating is shown in Figure 4.

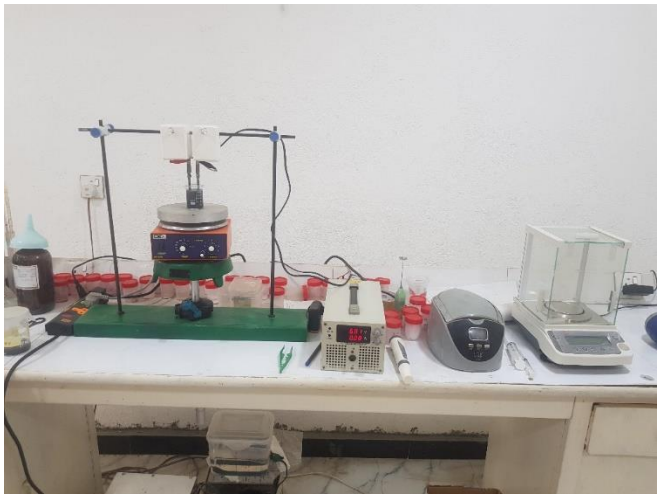

Figure 4. Electrophoretic deposition (EPD) system.

COATINGS CHARACTERIZATION

X-Ray Diffraction Test

The XRD test was conducted at the Development and Continuous Education Centre/The University of Baghdad-College of Education (Ibn Al-Haitham) (type XRD-6000 Shimadzu) for the substrate alloy and HAp-Gr coatings. The diffractograms were obtained using an X-ray diffractiometer. The XRD generator with Cu aimed at 40 kV and 30 mA, scanning speed 5°/minute was utilized. The scanning range was 30° to 80°.

Scanning Electrons Microscopy (SEM)

A scanning electrons microscope (SEM) was utilized to obtain surface composition and morphology. The specimen is imaged through a high-pack of electrons. Before the observation, the specimens were coated with a layer of gold around 15 nm (model Q150T, QUORUM) to prevent specimen charging throughout imaging. This test was done at the University of Babylon-Pharmacy College by using SEM type (TESCAN S8000) (Figure 3b).

Corrosion Test

The corrosion behaviour of the uncoated and coated specimens with HAp and HAp-Gr was investigated using Hank's solution. Table 3 [17] provides an illustration of the solution in Hank's chemical composition. The solution was created by adding the adequate amount of every ingredient to a litre of deionized water and stirring with a magnetic stirrer for about half an hour at room temperature.

Table 3. Chemical composition of Hank's solution [17].

No.	Constituents	(g/L)
1	NaCl	8
2	$CaCl_2$	0.14
3	KCl	0.4
4	$NaHCO_3$	0.35
5	Glucose	1
6	$MgCl_2.6H_2O$	0.1
7	$Na_2HPO_4.H_2O$	0.06
8	KH_2PO_4	0.06
9	$MgSO_4.7H_2O$	0.06

Open Circuit Potential (OCP)

The experiments were performed with the samples immersed in Hank's solution. A glass electrolytic cell with a capacity of 500 mL was employed. A saturated calomel electrode (SCE) is utilized to determine the working electrode voltage. Between the electrodes of reference and working one is where the voltmeter is linked. Open circuit potential measurements were taken for each specimen every 2 to 4 hours. The voltage was measured for the test duration at an interval of 1 second after the first value was recorded directly after the immersion (5 minutes), as shown in Figure 5.

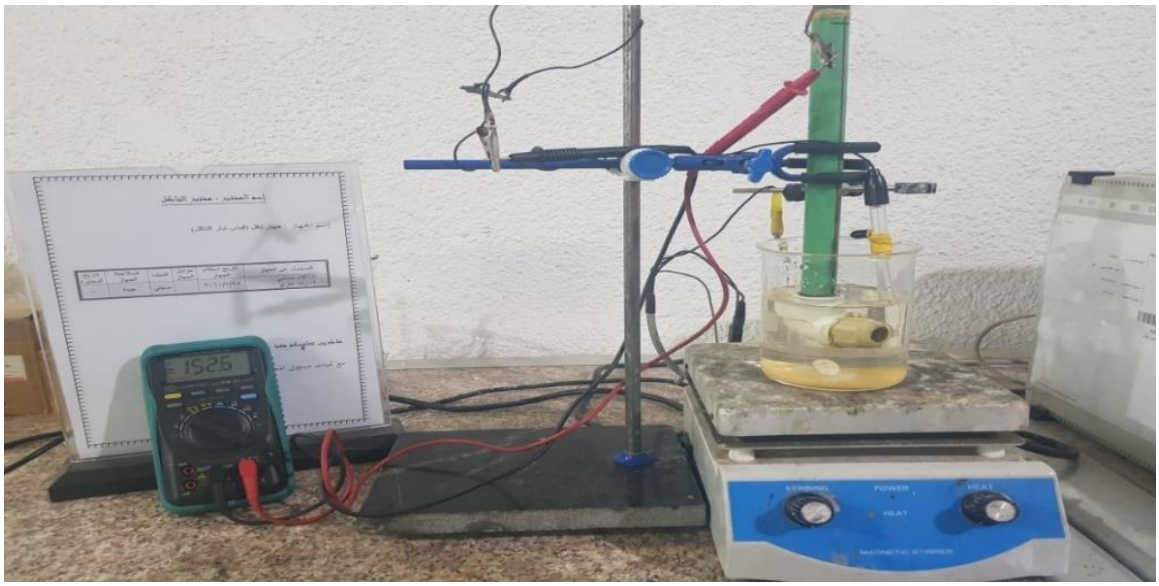

Figure 5. Schematic setup for measurement of open circuit potential.

Figure 6. The electrochemical system.

Potentiodynamic Polarization

Figure 6 shows the electrochemical test setup with three-electrode cells and electrolytes similar to those found in nature (Hank's solution). According to the American Society for Testing and Materials, the assistant electrode was Pt, the reference electrode was the SCE, and the working electrode was the sample. The corrosion current density ($I_{corr.}$) and corrosion potential ($E_{corr.}$) were computed using the Julius Tafel curve and polarization curves (cathodic and anodic branches). The test was initiated with a scanning rate of 0.4 mV/s from 300 mV below the OCP and proceeded up to 300 mV above the OCP.

The corrosion rate can be calculated using the equation below [18, 19].

$$\text{Corrosion Rate } (C_R) = \frac{8.76 \times 10^4 \times W}{A \times T \times D} \text{ (mm/y)} \quad (1)$$

where

mm/y = millimeter per year

W = loss in mass (g),

T = Duration of exposure (hours),

A = area (cm^2), and

D = density (g/cm^3).

Wear Test

The wet wear tests were studied by using micro-tester (pin-on-disk) type MT 4003 version 10, located in the Laboratories of the Department of Metallurgical Engineering/Babylon University; Hank's solutions are illustrated in Table 3 above at 37ºC, utilizing 150 rpm, and constant radius (6 mm) with various sliding loads and distance were 5, 10 and 15 N. Earlier starting the test, the sample is weighed utilizing a sensitive balance (0.0001). After the specific time (5, 10, 15, 20 and 25 minutes), the specimen test was weighed, and the volume loss was identified depending on formula (2). The test technique was covered based on ASTM G 99-05 [20].

$$\text{Volume loss} = \frac{\boldsymbol{weigth\ loss(g)}}{\rho(\frac{g}{cm^3})} \quad (2)$$

where:

Weight loss (g) = lost quantity after 5, 10, 15, 20, and 25 minutes.

ρ (g/cm^3) = theoretical density.

Adhesion Strength

Coating adhesion to the implantation surface is essential in medical uses, particularly for long-term use. The pull-off test was used to measure the adhesion strength between the coating and the alloy substrate for the samples coated with nano HAp and nano Hap–nano Gr, according to the ASTM-D4541 standard. The results show that nano Gr plays a significant role in coating adhesion to the substrate. To avoid any measurement errors, all coatings were deposited under identical conditions.

Contact Angle Studies

Contact angle measurements using Hank's solution were carried out for the Ti-13Zr-13Nb alloy, nano HAp, and nano Hap–nano Gr-(70 V) coatings. A contact angle goniometer (Zeiss, Germany) was used at room temperature. For each specimen, all measures were taken three times.

RESULTS AND DISCUSSION

Influence of Applied Voltage and Deposition Time on Coating

Figures 7 and 8 demonstrate the relationship between deposit weight, applied voltages, and time. The results show that with each applied voltage the weight of the deposition increases on the surface area of the sample at a fixed deposition time (7 minutes), but a decrease in the deposition weight for all voltages was observed when coating with the suspension solution (nano Hap + nano Gr coating) when compared to coating with the suspension solution (nano Hap coating). It was noted that the all curves increased (i.e., the continuation of increasing the deposition weight on the surface area of the specimen with an increase in the applied voltage), where the addition of graphene (nano Gr) led to the continued increase of the layer of coating deposited on the surface of the sample with an increase in voltage but remains less than nano HAp coating, taking into consideration that the increase in the coating layer at high voltages can cause a decrease in the density of the coating layer which causes an increase in the porosity, and then a reduction in adhesion. Kumari et al. [21] also proves it (according to the application of implanted inside the human body)..

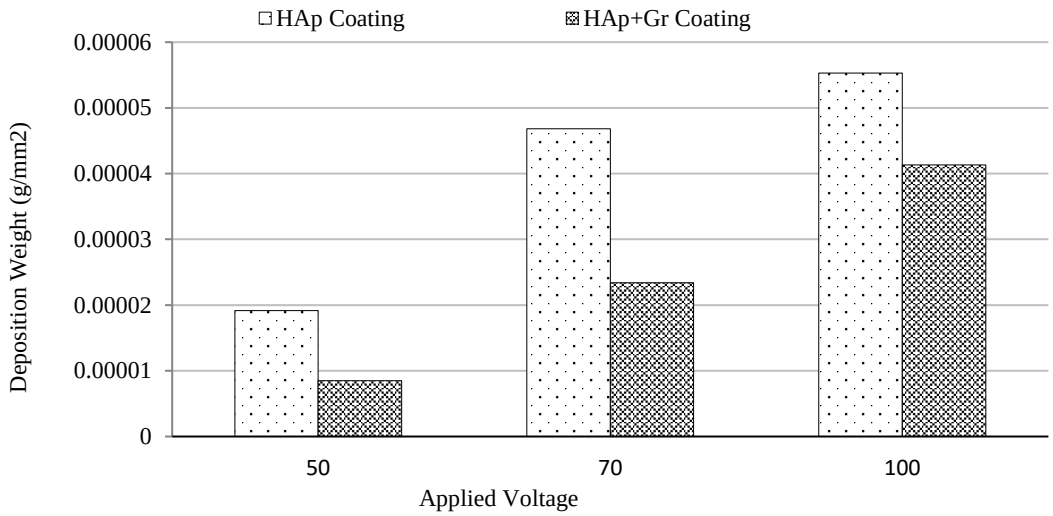

Figure 7. Influence of voltage on ethanol deposition weight for two types of coating and different voltages at 7 minutes.

The effect of time as a function of deposition weight shows increase in the deposition weight on the surface area of the sample with an increase in the deposition time at a constant voltage (70 V) for all coatings (nano HAp and nano Hap + nano Gr). The addition of graphene (nano-Gr) to the coating (nano-HAp) leads to a decrease in the curved rise with the increase in the deposition duration (i.e., it is possible to reach the saturation state with an increase in deposition time at constant voltage), as opposed to coating without adding graphene which will continue to rise. At a constant voltage, it is expected that the potential variance between the electrodes will be kept constant, so the electric field affects the trip of the ions to the sample's surface with the deposition time since the creation of an insulating particles layer on the electrode's surface. From this, we can conclude that the effect of stress when adding graphene is greater than the effect of time at the same addition (Figure 8).

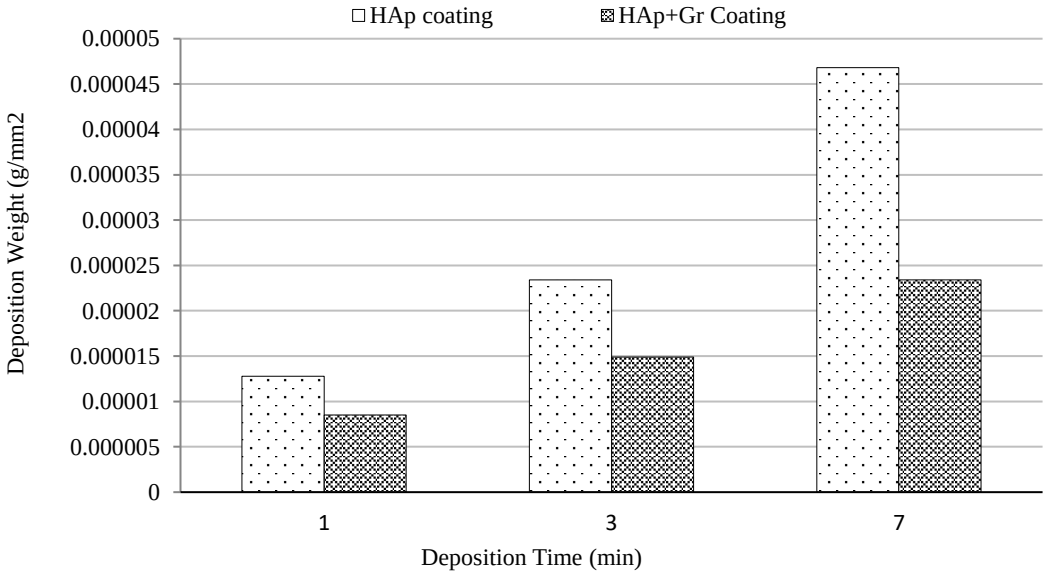

Figure 8. Effect of time on ethanol deposition weight for two coating types at the applied voltage of 70 V.

It is clear from the above figures that the thickness and amount of deposition can easily be governor either by varying the applied voltages or the deposition time. The combination of these factors could be

utilized to obtain the preferred thickness and mass, and the best adhesion and density of the coating layer. Adding graphene to the coating solution leads to having a coating layer with less thickness compared to the solution without adding it; at 70 V and 1, 3 and 7 minutes, the thickness of the solution with adding graphene was 49.2, 64.5, and 70.1 while it was 58.3, 75.6, and 71.9, respectively, for the same conditions without adding it.

At 7 minutes and 50, 70, and 100 V, the layer thickness was 60.9, 62.7, and 79.3 and 71.6, 78.2, and 83.8, with and without addition of graphene, respectively. Figure 9 shows the microstructure of the thickness layer.

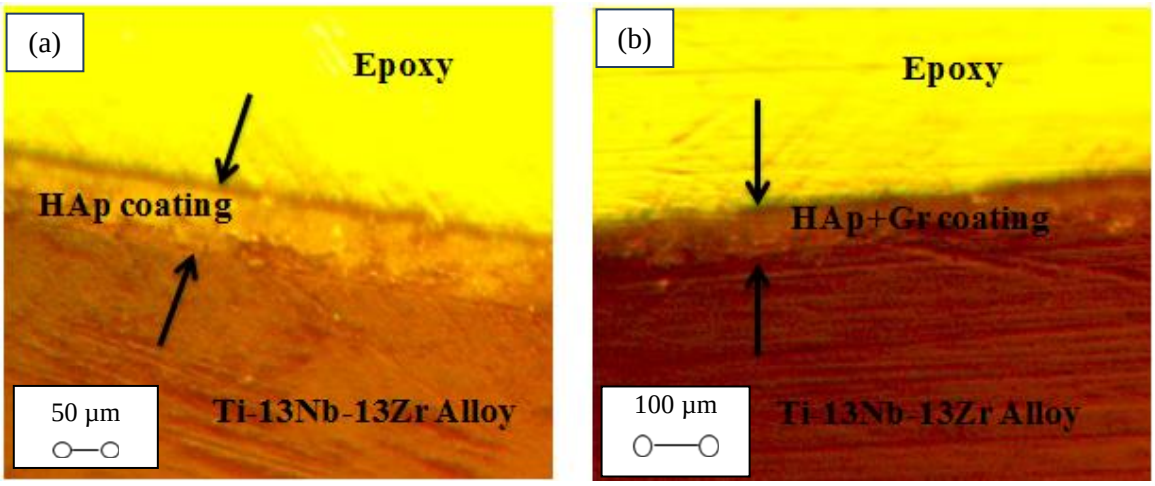

Figure 9. Optical microscopy pictures of (a) HAp coating; (b) Hap + Gr coating at 70 V for 7 minutes. Gr, graphene; HAp, hydroxyapatite.

Surface Morphology Analysis

SEM images for the surface morphology of coated specimens with graphene and HAp at various magnifications are shown in Figure 10A. As shown in Figure 10B, the number of microcracks present on the surface of the HAp coating is reduced when graphene nanoparticles are added. Furthermore, no surface flakes or cracks have been detected on the surface of the graphene coating, which can be seen on the surface of the HAp, and the higher roughness of the graphene coating can be observed compared to the HAp coating. These cracks can be attributed to high ethanol evaporation and quick drying of the coatings due to the formation of thermal stresses caused by the variance in thermal expansion of the HAp coating and the base alloy, which is one of the most important causes of cracks on the coating's surface.

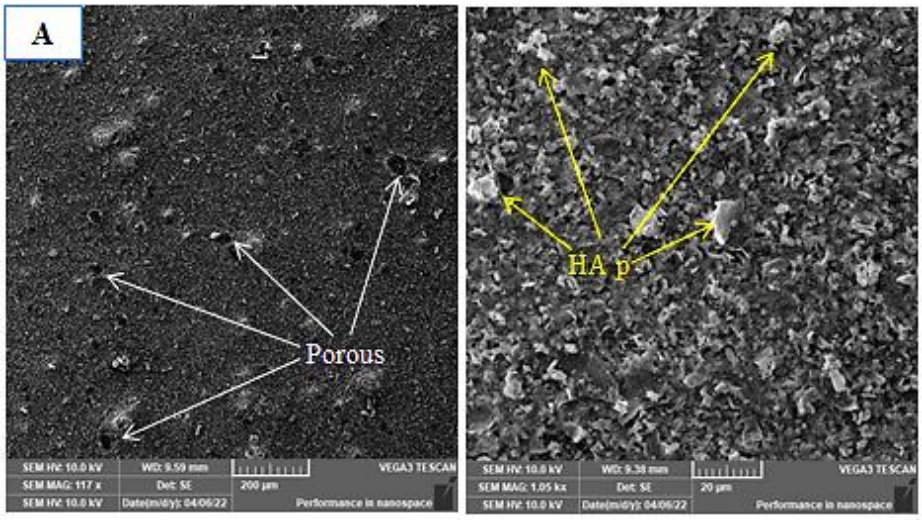

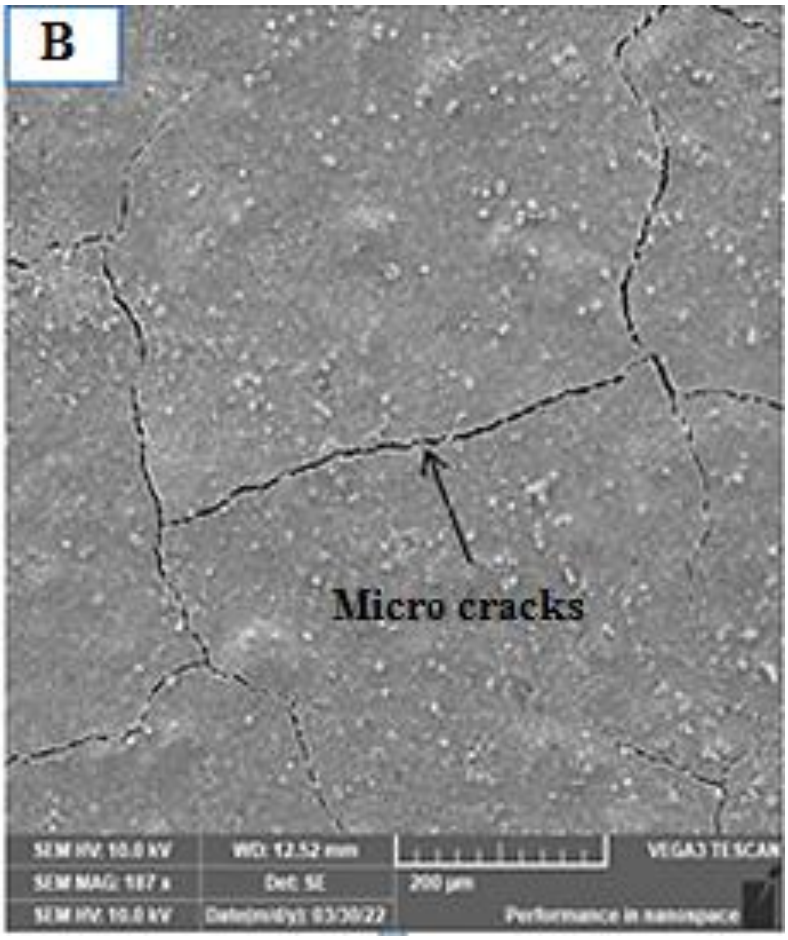

Figure 10. Scanning electron micrographs showing coating surface morphology of (A) graphene (Gr) coating, (B) hydroxyapatite (Hap) coating deposited by electrophoretic deposition at 70 V for 7 minutes.

X-Ray Diffraction Analysis

Figure 11 demonstrates the X-ray diffraction (XRD) patterns of HAp-coated Ti-13Nb-13Zr alloy at 70 V and 7 minutes. The XRD patterns were almost similar to HAp-coated Ti-13Nb-13Zr alloy with graphene. The XRD patterns revealed the density of the Ti-13Nb-13Zr alloy peaks compared to HAp, which is attributed to the relatively low coating thickness, which allows the X-rays to penetrate the surface of the substrate alloy.

Wetting Behavior

Measurements of contact angle were done as a function of deposition time and applied voltage for nano HAp, nano HAp + nano Gr in ethanol solution at 70 V and a range of deposition times. From the result, the contact angle decreases with increasing deposition time; the lowest contact angle values, approaching 20° after 7 minutes of deposition, are shown by nano HAp suspension coatings. Notably, the contact angles advanced during the drying process, which was influenced by the presence of cracks. The wettability of coated specimens is further affected by surface roughness, topography, and porosity.

As seen in Figure 12, the surface hydrophilicity of non-coated and coated specimens differed significantly. Compared to the coated samples, the non-coated (base sample) surface had an upper aqueous contact angle of 54°, representing a less hydrophilic surface. It should be mentioned that increasing deposit duration leads to decrease in contact angle until the drop became more splayed over the surface, indicating high absorption. The same result above was also noted in different percentages with graphene addition. Taking into consideration, the contact angle was measured with Hank's solution.

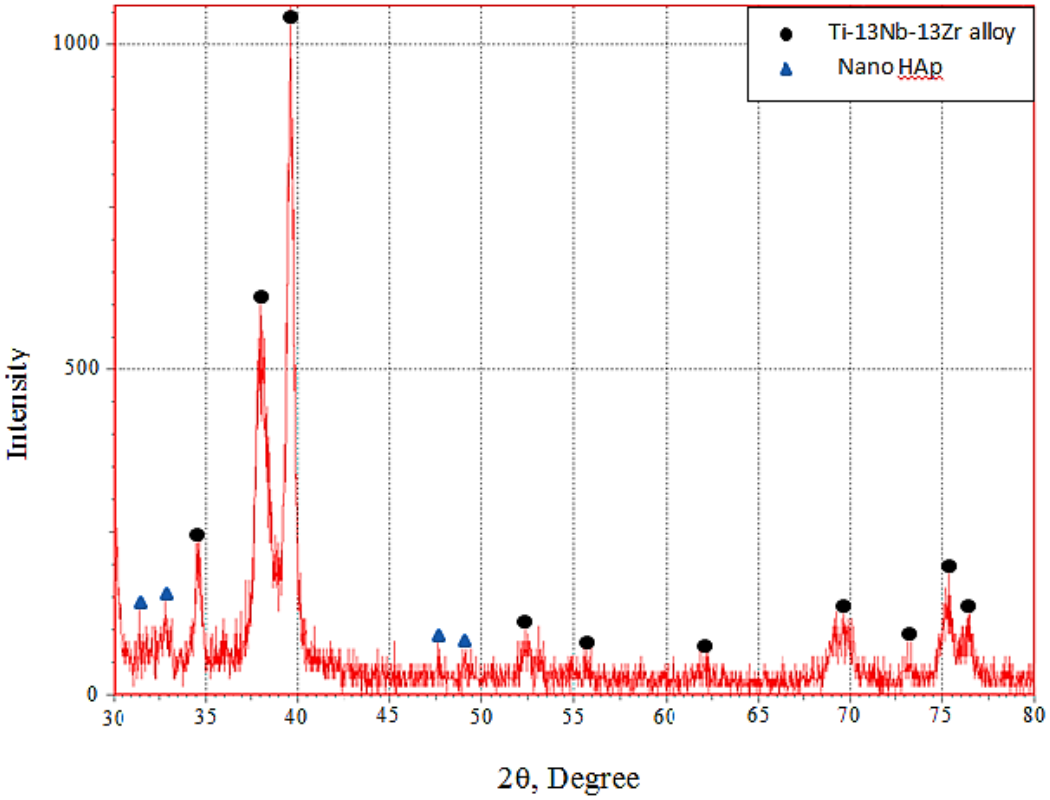

Figure 11. X-ray diffraction (XRD) patterns of nano HAp coating.

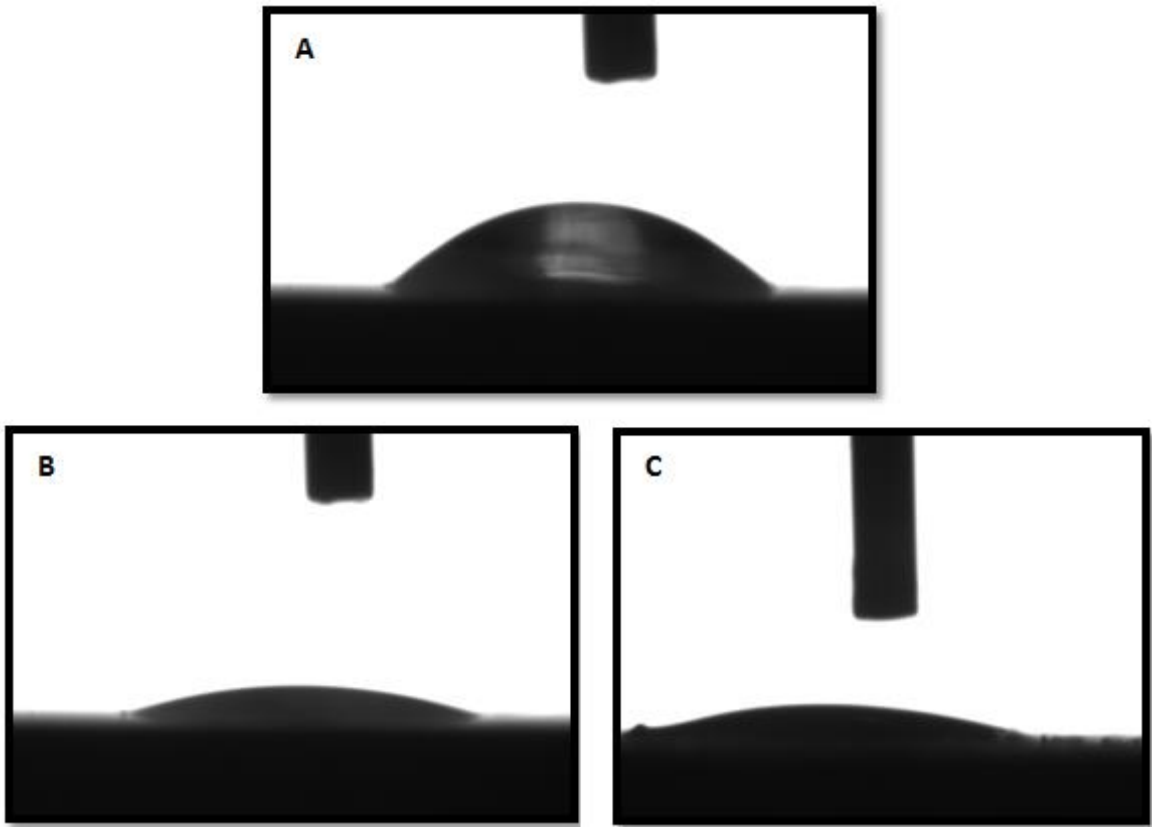

Figure 12. Contact angle measurements with Hank's solution of (a) non-coated sample (base), (b) coated sample (nano Hap + nano Gr coating), and (c) (nano Hap coating).

Adhesion Test

According to the results of the pull-off test, the bonding strength of nano HAp coating is 0.91 MPa, which by addition of graphene, increases to 3.03 MPa in HAp-0.06Gr, for the same condition (voltage and deposition time). Therefore, Gr enhances the HAp coating adhesion to the Ti-13Nb-13Zr substrate. The existence of cracks is the primary cause of poor adhesion coating. In addition, adhesion test results on several sets of coatings showed that adhesion strength reduces as the voltage and time used for coating increase. Increasing the voltage increases the chances of crack formation and lowers the density.

Corrosion Test

The corrosion behavior of all the utilized alloys was studies in Hank's solution. The corrosion considerations are corrosion rate, corrosion potential ($E_{corr.}$), and corrosion current density ($I_{corr.}$) resulting from the corrosion check for the samples solutions at 37°C.

The results presented in Table 4 show a major and excellent improvement in resistance against corrosion of Ti-13Nb-13Zr alloy with (nano Hap + nano Gr) coating (95%, 89%) for (1 and 7 minutes) respectively, and the $I_{corr.}$ of these alloys ranged between 1.821 μA/cm^2 and 2.976 μA/cm^2. It could be noted that the I_{corr} of Ti-13Nb-13Zr alloys with nano Hap + nano Gr coating is lower than that for each with nano HAp coating and without coating. However, the $E_{corr.}$ values for Ti-13Nb-13Zr alloys with nano Hap + nano Gr coating are –0.112 and –0.159 mV for 1 and 7 minutes, respectively, which are less than with nano HAp coating and without coating.

Table 4. Corrosion current density ($I_{corr.}$), corrosion potential ($E_{corr.}$), and corrosion rate for all alloys in Hank's solution at 37°C.

Parameters	Substrate Uncoating	(nanoHAp)-coating		(nanoHAp + nanoGr)-coating	
		1 min	7 min	1 min	7 min
$I_{corr.}$ (μA/cm^2)	6.998	2.762	3.44	1.821	2.976
E (mV)	-0.245	-0.130	-0.199	-0.112	-0.159
Corrosion rate	0.871	0.212	0.836	0.041	0.383
Improvement %	-------	76%	74.6%	95%	89%

Figure 13 shows that uncoated titanium substrates have reduced resistance against corrosion when determined by corrosion current density. The resistance against corrosion of titanium alloys with deposited nanoHAp and nanoHAp + nanoGr coatings was studied, and it was found to be often superior to that of an uncoated substrate. Corrosion increased in both coatings at 7 minutes compared to 1 minute, most likely due to their porous structure and thickness, resulting in the development of some corrosion channels and the presence of localized corrosion. The rate of corrosion, on the other hand, is still very low. Also, compared to all coatings, the corrosion potentials for the uncoated Ti13Zr13Nb control specimen were the highest.

Wear Test

From Figure 14, it is possible to note the relative stability of volume loss of graphene coating (especially at 1 min and 10 N) on Ti-13Nb-13Zr alloys; this indicates the complete protection of the loaded layer over time compared to Ti-13Nb-13Zr alloy uncoated and HAp coatings (at 1 and 7 minutes at the same load). This is attributable to the hardness of this coating, which is difficult to remove over time, so it is subjected to Archard's law which states that weight loss for materials is inversely related to the material hardness magnitude [22]. In addition, the high adhesion of this layer makes it more stable and cohesive on the Ti-13Nb-13Zr alloy surface [23, 24].

Conversely, the nanoHAp coatings at 1 and 7 minutes shows increasing volume loss to all load if it is compared to nanoHAp + nanoGr coating at 1 and 7 minutes. Since the hardness of this coating decreases compared to other coatings, one can easily remove these layers from the surface of the alloy.

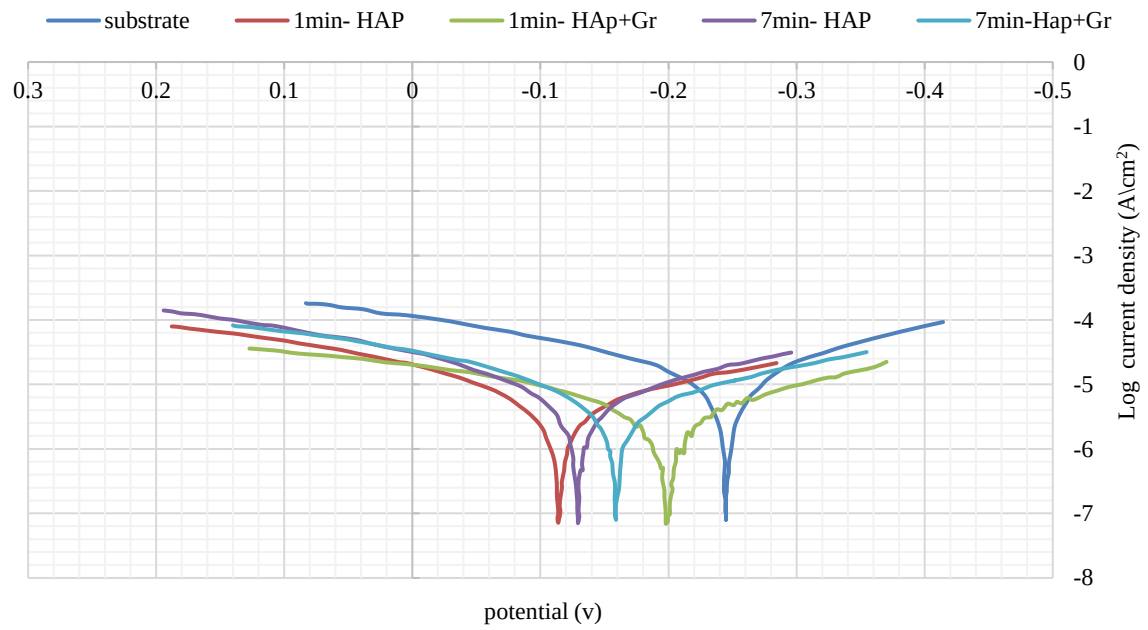

Figure 13. Potentiodynamic polarization curves of nanoHAp, nanoHAp + nanoGr coatings and reference specimen Ti13Zr13Nb in Hank's solution at 37°C at the same voltage 70 V.

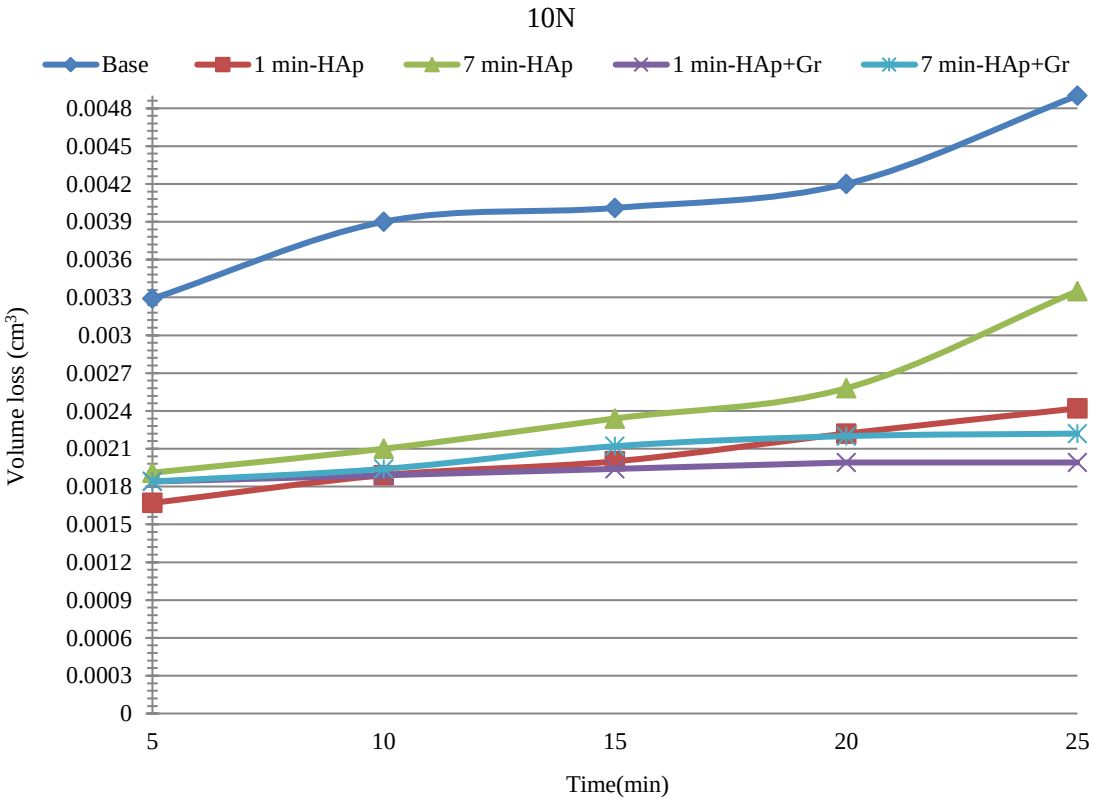

Figure 14. Volume losses versus time for base specimen, HAp, and Hap + Gr alloys under 10 N load.

The microstructure in Figures 15a and 16b show the morphology of the worn surface of the tested specimens, where the wear evidence could be detected on the worn surfaces of all the alloys. The wear areas and plastic deformation could be detected on the wear tracks that resulting from the solid abrasive ball penetration to the coating surface. The penetration depth depends on time, load and the hardness of the tested coating.

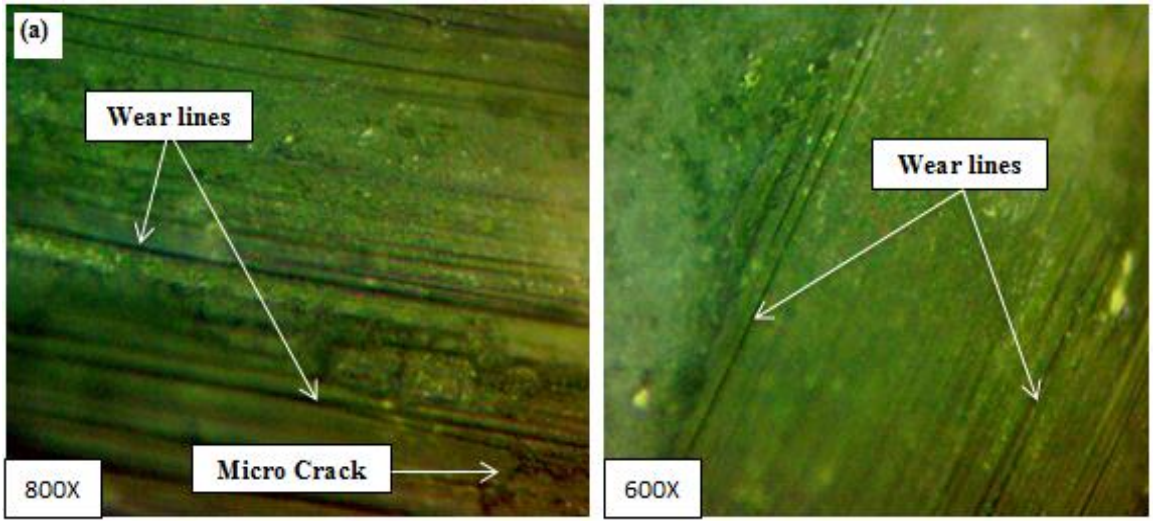

Figure 15. Microstructure for nanoHAp coating by use (light optical microscope) after wear test under 10 N load at 7 minutes and 70 V.

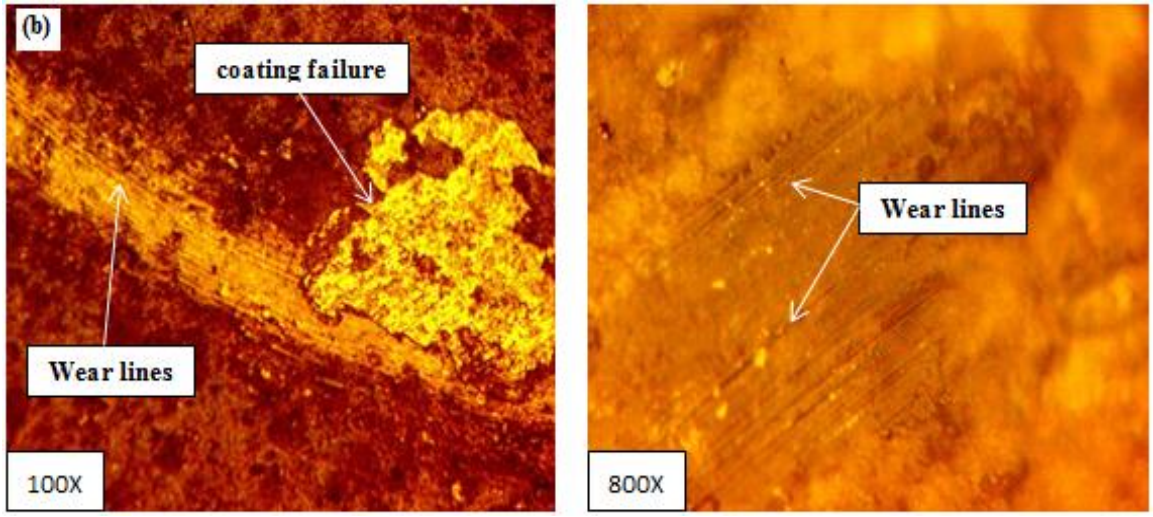

Figure 16. Microstructure for nanoHAp + nanoGr coating by use (light optical microscope) after wear test under 10 N load at 7 minutes and 70 V.

CONCLUSIONS

From the study, the following conclusions may be drawn:

1. The electrophoretic method is an excellent alternative to coating materials such as polymeric, ceramic, and glass, particularly for biomedical applications.
2. Improving the quality of the coating layer depends mainly on the suspension solution and the materials added to it that make the coating layer more receptive to the surface of the sample, and this was proven by adding chitosan and graphene, not to mention the parameters of the coating method, which also have a substantial effect on the coating quality.
3. The addition of graphene led to clear stability of the deposited weight with increasing time, in contrast to an increase in applied voltage, which led to the deposition of a thinner layer of the coating compared to the coating layer without adding graphene, thus reducing cracks and pores that may lead to the destruction of the layer.
4. The number of microcracks on the surface of the hydroxyapatite coating is reduced when graphene nanoparticles are added. Furthermore, no surface flakes or cracks have been detected

on the graphene coating surface, which can be seen on the surface of the hydroxyapatite.
5. The addition of graphene made the layer of coating deposited on the sample's surface more biocompatible, as it was proven that the surface of the layer was more hydrophilic when compared to the hydroxyapatite layer and the base sample without coating.
6. The cracks and less dense coating layers have lower adhesion strength values.
7. Remarkable enhancement in the corrosion resistance was observed on adding graphene comparison with the coating layer without adding graphene and the base alloy without coating.
8. The hardness of the graphene layer made it a non-scratchable layer compared to the hydroxyapatite layer.

From the preceding, it can be proven that graphene is a biomaterial with excellent biocompatibility within the human body.

Acknowledgements

The authors would like to thank the Department of Metallurgical Engineering/Faculty of Materials Engineering/Babylon University for their assistance with this project.

REFERENCES

1. Fitriyana DF, Nugraha FW, Laroybafih MB, Ismail R, Bayuseno AP, Muhamadin RC, Siregar JP. The effect of hydroxyapatite concentration on the mechanical properties and degradation rate of biocomposite for biomedical applications. IOP Conf Ser Earth Environ Sci. 2022; 969 (1): 012045.
2. Nicholson JW. Titanium alloys for dental implants: a review. Prosthesis. 2020; 2 (2): 100–116.
3. Kumar P, Mahobia GS, Singh V, Chattopadhyay K. Lowering of elastic modulus in the near-beta Ti–13Nb–13Zr alloy through heat treatment. Mater Sci Technol. 2020; 36 (6): 717–725.
4. Ossowska A, Zieliński A, Olive JM, Wojtowicz A, Szweda P. Influence of two-stage anodization on properties of the oxide coatings on the Ti–13Nb–13Zr alloy. Coatings. 2020; 10 (8): 707.
5. Amani H, Arzaghi H, Bayandori M, Dezfuli AS, Pazoki-Toroudi H, Shafiee A, Moradi L. Controlling cell behavior through the design of biomaterial surfaces: a focus on surface modification techniques. Adv Mater Interfaces. 2019; 6 (13): 1900572.
6. Hu S, Li W, Finklea H, Liu X. A review of electrophoretic deposition of metal oxides and its application in solid oxide fuel cells. Adv Colloid Interface Sci. 2020; 276: 102102.
7. Akhtar MA, Mariotti CE, Conti B, Boccaccini AR. Electrophoretic deposition of ferulic acid loaded bioactive glass/chitosan as antibacterial and bioactive composite coatings. Surf Coatings Technol. 2021; 405: 126657;.
8. Sikkema R, Baker K, Zhitomirsky I. Electrophoretic deposition of polymers and proteins for biomedical applications. Adv Colloid Interface Sci. 2020; 284: 102272.
9. Venkatesan J, Anil S. Hydroxyapatite derived from marine resources and their potential biomedical applications. Biotechnol Bioprocess Eng. 2021; 26 (3): 312–324.
10. Sivasankari S, Kalaivizhi R, Gowriboy N, Ganesh MR, Shazia Anjum M. Hydroxyapatite integrated with cellulose acetate/polyetherimide composite membrane for biomedical applications. Polym Composites. 2021; 42 (10): 5512–5526.
11. Rashad M, Pan F, Tang A, Lu Y, Asif M, Hussain S, Mao J. Effect of graphene nanoplatelets (GNPs) addition on strength and ductility of magnesium-titanium alloys. J Magnesium Alloys. 2013; 1 (3): 242–248.
12. Huang SM, Liu SM, Ko CL, Chen WC. Advances of hydroxyapatite hybrid organic composite used as drug or protein carriers for biomedical applications: a review. Polymers. 2022; 14 (5): 976.
13. Nesovic K, Abudabbus MM, Rhee KY, Miskovic-Stankovic V. Graphene based composite hydrogel for biomedical applications. Croat Chem Acta. 2017; 90 (2): D1.
14. Bartmanski M, Cieslik B, Glodowska J, Kalka P, Pawlowski L, Pieper M, Zielinski A. Electrophoretic deposition (EPD) of nanohydroxyapatite-nanosilver coatings on Ti13Zr13Nb alloy. Ceram Int. 2017; 43 (15): 11820–11829.
15. Moskalewicz T, Zimowski S, Zych A, Łukaszczyk A, Reczyńska K, Pamuła E. Electrophoretic deposition, microstructure and selected properties of composite alumina/polyetheretherketone

coatings on the Ti-13Nb-13Zr alloy. J Electrochem Soc. 2018; 165 (3): D116.
16. Singh S, Singh G, Bala N. Electrophoretic deposition of hydroxyapatite-iron oxide-chitosan composite coatings on Ti–13Nb–13Zr alloy for biomedical applications. Thin Solid Films. 2020; 697: 137801.
17. Abd Alkadim NM, Salman JM. Study the corrosion behavior and microstructure of Ti-5Al-2.5 Fe-xMo alloys for biomedical applications. ARPN J Eng Appl Sci. 2019; 14 (1): 227–239.
18. Haruna K, Saleh TA. N,N′-bis-(2-aminoethyl) piperazine functionalized graphene oxide (NAEP-GO) as an effective green corrosion inhibitor for a simulated acidizing environment. J Environ Chem Eng. 2021; 9 (1): 104967.
19. Singh A, Dayu X, Ituen E, Ansari K, Quraishi MA, Kaya S, Lin Y. Tobacco extracted from the discarded cigarettes as an inhibitor of copper and zinc corrosion in an ASTM standard D1141-98 artificial seawater solution. J Mater Res Technol. 2020; 9 (3): 5161–5173.
20. ASTM. Standard Test Method for Wear Testing with a Pin-on-Disk Apparatus. Wear. 2010; 5: 1–5.
21. Kumari S, Tiyyagura HR, Pottathara YB, Sadasivuni KK, Ponnamma D, Douglas TEL, Skirtach AG, Mohan MK. Surface functionalization of chitosan as a coating material for orthopaedic applications: a comprehensive review. Carbohydr Polym. 2021; 255: 117487.
22. Cvijović-Alagić I, Cvijović Z, Mitrović S, Panić V, Rakin M. Wear and corrosion behaviour of Ti–13Nb–13Zr and Ti–6Al–4V alloys in simulated physiological solution. Corros Sci. 2011; 53 (2): 796–808.
23. Kumbhalkar MA, Rangari DT, Pawar RD, Phadtare RA, Raut KR, Nagre AN. Finite element analysis of knee joint with special emphasis on patellar implant. In: Akinlabi E, Ramkumar P, Selvaraj M, editors. Trends in Mechanical and Biomedical Design. Lecture Notes in Mechanical Engineering. Singapore: Springer; 2021. pp. 319–333. doi: 10.1007/978-981-15-4488-0_29
24. Kumbhalkar MA, Rambhad KS, Nand Jee K. An insight into biomechanical study for replacement of knee joint. Mater Today Proc. 2021; 47 (Part 11): 2957–2965. doi: 10.1016/j.matpr.2021.05.202.

